The Forced Annual Reversal of the Atlantic North Equatorial Countercurrent[1]

SILVIA L. GARZOLI AND ELI J. KATZ

Lamont-Doherty Geological Observatory of Columbia University, Palisades, NY 10964

(Manuscript received 31 March 1983, in final form 28 June 1983)

ABSTRACT

We analyze the variability of the thermal structure associated with the Atlantic North Equatorial Countercurrent (NECC) and its relation to the seasonally varying winds. The analysis performed allows us to establish the period of time and the region where the NECC reverses direction. West of 25°W, the depth of the thermocline in the southern side of the NECC (4 to 7°N) annually oscillates 180° out of phase to the oscillations on the northern side (7 to 10°N). East of 25°W the thermocline rises and falls nearly in phase across the countercurrent. If the flow can be uniquely presumed from the thermal structure, the NECC disappears during the boreal spring in the western basin. The reversal of phase from north to south over one part of the ocean, but not the other, is shown to be mirrored in the annual variation of the curl of the stress induced at the surface by the winds. In order to quantify this result, the different terms of the vorticity equation are calculated from the data. We conclude that those derived from the acceleration terms do not contribute significantly to the thermocline displacement anywhere in the region of the NECC and that in the interior of the basin, the reversal of the trade winds is responsible for the reversal of the NECC through the combined mechanisms of local Ekman pumping and the divergence of the geostrophic currents.

1. Introduction

A major component of the current system in the equatorial Atlantic is the North Equatorial Counter-current (NECC) that generally flows eastward between 3 and 10°N counter to the trade winds. It is positioned between two westward flows: the North and South Equatorial Currents. The most extensive direct measurement of the NECC was made during the GATE experiment (1974) at five current meter moorings along 23.5°W. The resulting three-month average of the zonal velocity (Bubnov and Egorikhin, 1979) is reproduced in Fig. 1.

Evidence of the NECC, besides ship drift data, is based almost entirely on the strong meridional slope of the shallow thermocline observed in hydrographic data (also Fig. 1). It is widely assumed that the current is nearly in geostrophic balance, and indeed velocities and transport so calculated are in coarse agreement with what has been observed. A limited but convincing demonstration of geostrophy has been made by D. Halpern (personal communication, 1983) in the physically similar central Pacific Ocean. In the present work, changes in the meridional slope of the thermocline are implicitly interpreted as reflecting changes in the transport of the NECC.

The NECC is subject to seasonal changes. There is some evidence that those changes include the disappearance of the NECC. Ship drift measurements

(P. L. Richardson, personal communication, 1983) show an eastward current in summer and fall and a westward current in winter and spring in the western Atlantic. This variation also depends on longitude. East of 25°W the ship drift measurements indicate year-round eastward velocities. The reversal in direction of the mixed-layer flow in the region of the NECC (by definition, eastward) is independently demonstrated by a collage of three unpublished drifting buoy tracks (Fig. 2). One objective of this paper is to show that these near-surface observations are consistent with the slope of the thermocline "across" the NECC.

Most theoretical studies approach the problem of modeling the physical processes that govern the variability of large-scale, low-frequency tropical currents by a two or more layer, reduced-gravity, linear transport model on a β-plane (see, e.g., McCreary, 1976; Busalacchi and O'Brien, 1980; Cane and Sarachik, 1981; etc.) In these models it is assumed that at some depth beneath the upper layer the horizontal pressure gradient is zero. The interface between two appropriate layers is defined as the depth of the thermocline.

From the equations of motion for such a system (see Section 3) we can easily deduce the vorticity equation which gives us a convenient relation for the displacement of the thermocline. When independently equated to the rhs of the equation, the first term is the divergence set up at the surface by the wind stress due to Ekman pumping and the second term is the planetary geostrophic divergence (or the divergence of the geostrophic transport) inherent in a rotating sphere. Both processes result in vertical displacement of the thermocline.
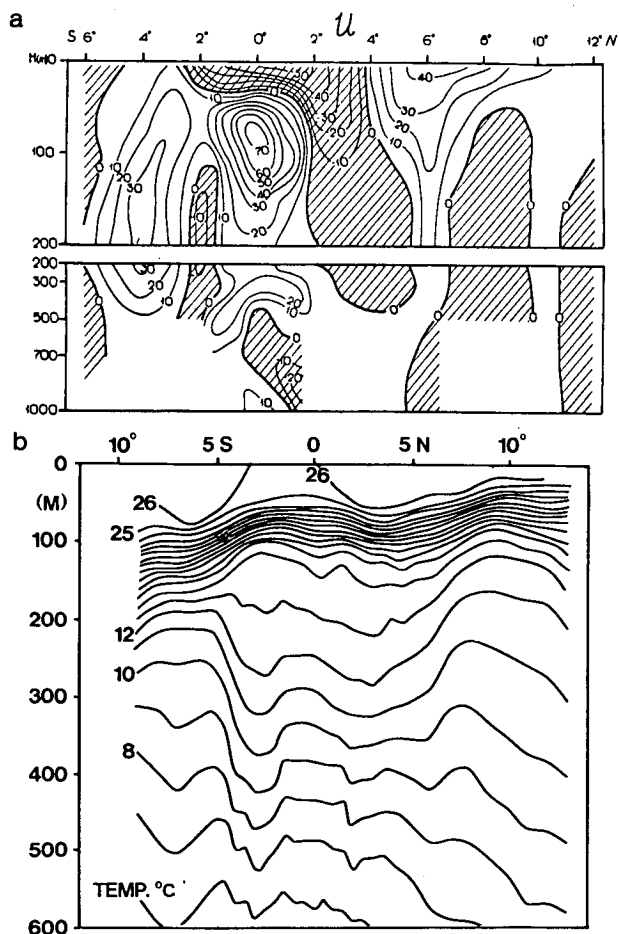
FIG. 1. (a) The mean zonal currents across 23.5°W from direct measurements during GATE (July–September, 1974) north of 2°S and from geostrophic calculations south of 2°S (after Bubnov and Egorikhin, 1979). (b) The mean temperature field from measurements by the R.V. *Trident* and Akad. *Semen Dezhnev* during the same time period.

At midlatitudes it has been demonstrated that at seasonal time scales these two terms are dominant. The resulting equation (in a reduced form that neglects the contribution related to the acceleration terms) has been analyzed during the last decade in several studies to explain the seasonal variability of tropical and subtropical currents in the Pacific Ocean (i.e., Meyers, 1975, 1979; McCreary, 1976; White, 1977, 1978). For the Pacific North Equatorial Current, Meyers (1975) finds that most of the temporal variations in the meridional slope of the thermocline could be accounted for by meridional variations in the Ekman pumping. White (1977) used the same data set as Meyers and concluded that the depth of the main thermocline fluctuated not only in response to local wind-stress curl, but also in response to westward propagating baroclinic planetary (Rossby) waves of a one-year period which emanated from the eastern boundary.

In the tropical North Pacific Ocean, Meyers (1979) analyzed a simple model which permits an oceanic response to Ekman pumping in the form of non-dispersive Rossby waves. Results are qualitatively consistent with the observed variations, but deficiencies of the model have been noted: the model produces variations which are too large at 6°N and also requires a larger-than-expected value of the nondispersive Rossby wave phase speed in order to correctly produce the observed variations at 12°N.

In the Atlantic, the mean and seasonally varying vertical velocity at the base of the Ekman layer were computed by Leetmaa and Bunker (1978) for the North Atlantic from 5 to 60°N. Using the same set of historical wind stress data, Hellerman (1980) calculates mass transports using the Sverdrup relation. Extremes in the seasonal cycle of mass transport in the Equatorial Countercurrent and North Equatorial Current regions are displayed and tabulated.

In a recent paper, Busalacchi and Picaut (1983) solve a numerical model incorporating a single baroclinic mode and a realistic coastline geometry to analyze the linear, dynamic response to estimates of the seasonal wind field over the tropical Atlantic Ocean. The western pycnocline fluctuations are described by an equation analogous to Eq. (1). Their results are compared with ours later in this paper.

In Section 2 we report the results of an extensive analysis of the historical ocean data in terms of the annual variability of the depth of the thermocline in the region 3°S to 10°N and 10°W to 48°W. The monthly and zonal change of the slope of the thermocline across the North Equatorial Countercurrent (NECC) (3 to 9°N) is compared to earlier studies and the direct observations mentioned above.
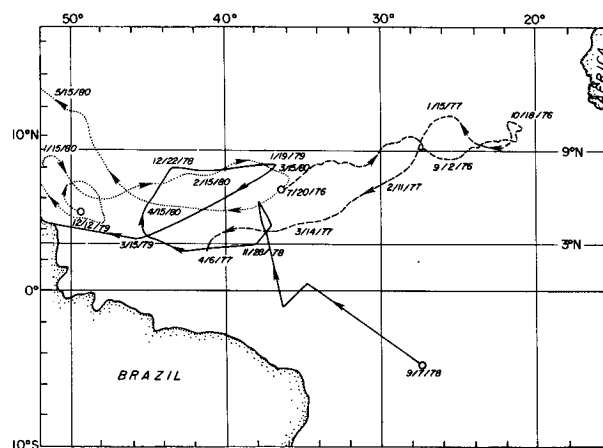

FIG. 2. Trajectories derived from three satellite-tracked drifting buoys launched within 30 m of the surface by: Cochrane (July 1976–April 1977, personal communication, 1982), Molinari (September 1978–March 1979, personal communication, 1982) and Klaus (December 1979–May 1980, Météorologie National Française, personal communication, 1982).

Next, we examine the balance of terms in the vorticity equation (Section 3) using only the thermocline depth and the wind stress field at an annual frequency. Both the overall balance and the relative importance of the individual terms are described as a function of location in the basin.

2. Analysis of the data

a. Data sources

Two different sets of data have been analyzed to study the thermocline response to the seasonally varying winds in the region of the NECC (48 to 10°W, 3 to 9°N): 1) the Bureau Nationale des Données Oceanographiques file of temperature versus depth as created by J. Merle from all available data up to 1974, supplemented where necessary by available data from subsequent years and 2) the wind stress file provided by Hellerman and created from the National Climate Center (TDF-11) tape containing shipboard wind observations for the period 1941–72.

The depth of the thermocline is defined as the depth of the maximum gradient (which is taken as the mean depth in the depth interval of the maximum temperature gradient between standard hydrographic depths). This method is used in the absence of a single isotherm characteristic of the thermocline across the entire basin. Data have been averaged in 2° × 2° boxes at every degree in latitude and every two degrees in longitude.

The standard error of the monthly-mean depth of each area is typically between 1 and 4 m. Certain months, particularly December and January, are often inadequately sampled and their values are obtained by a regression analysis which fits an annual cycle to the available data. The standard deviation of the monthly-mean values to the annual cycle generally lie between 7 and 13 m. If we can assume that the error associated with a depth estimate from the annual fit decreases with the square root of the number of observations (i.e., monthly-mean depths), then the combined uncertainty of a thermocline depth will range between 3 and 8 m.

The vertical component of curl τf^{-1} is obtained with a 2° × 2° resolution, and the same analysis was performed to the calculated curl τf^{-1} to make both sets of data analogous.

b. The thermal structure

The annual mean of the depth of the thermocline as defined above is shown in Fig. 3a. After removing the annual mean, the dominant signal remaining is an annual cycle. The amplitude and phase of this cycle are shown in Figs. 3b and c. The shaded areas indicate the areas where the data are not well represented by an annual cycle. The amplitude plot (Fig. 3b) shows

decreasing values towards the east and a zonal band of maximum values near 4°N. The phase diagram (Fig. 3c) shows that there is not much phase change between the equator and roughly 7°N, but there is a well-defined change of 180° above it for most of the western and central third of the basin. By 20°W there is no phase change.

This difference in phase change of the annual signal across the NECC is illustrated in the next figure. Fig. 4 compares the annual variation of thermocline depth in the zonal bands 41–45°W and 17–21°W. The reverse of the annual cycle at 41–45°W has a pronounced pivoting point at 6°N. At 17–21°W there is no reversal.

As mentioned in the Introduction, the variability of the NECC is associated with a strong meridional slope of the isopycnals and therefore of the isotherms. Fig. 5 shows the difference of the thermocline depth across the NECC as a function of time and longitude. Differences were obtained from the annual fits at 30°N and 9°N. This figure summarizes the above results and is convenient for comparing with earlier studies (Katz, 1981, and Merle, 1978) and with the surface velocities in Fig. 2. In the east (15–25°W) there is little seasonal variation, and a weak NECC associated with a 20-m deepening of the thermocline will be present all year. In the central region (25–35°W) we expect a doubling of the current in the boreal fall compared to the east, but a weakening to near zero in the spring. The synoptic sections of dynamic height previously analyzed by Katz consisted primarily of data from this central region and evidenced this type of seasonal behavior. Twenty-two Soviet sections along 30°W (Belevich et al., 1979) show reduced geostrophic transport between March and July with near zero flow in May.

In the western sector (35–45°W) the seasonal variation is most pronounced. The fall thermocline displacement doubles again (at its maximum) relative to the east and reverses in the spring to a negative displacement of greater than 20 m over half of the region. The reversal of the NECC was not reported by Merle (1978) who only contrasted the seasonal differences between summer and winter.

These results can be compared with those obtained theoretically by Busalacchi and Picaut (1983). A linear, single baroclinic-mode, numerical model on an equatorial β-plane is used to study the oceanic response to an applied wind stress forcing. The simulated NECC undergoes significant spatial and temporal variations, but the reversal of the current is not reproduced. Within the region 3–9°N and 30–42°W the NECC is strongest in August and is non-existent in April.

3. The vorticity equation

The vertically averaged equations for the response of a two-layered ocean to wind forcing in the β-plane are:
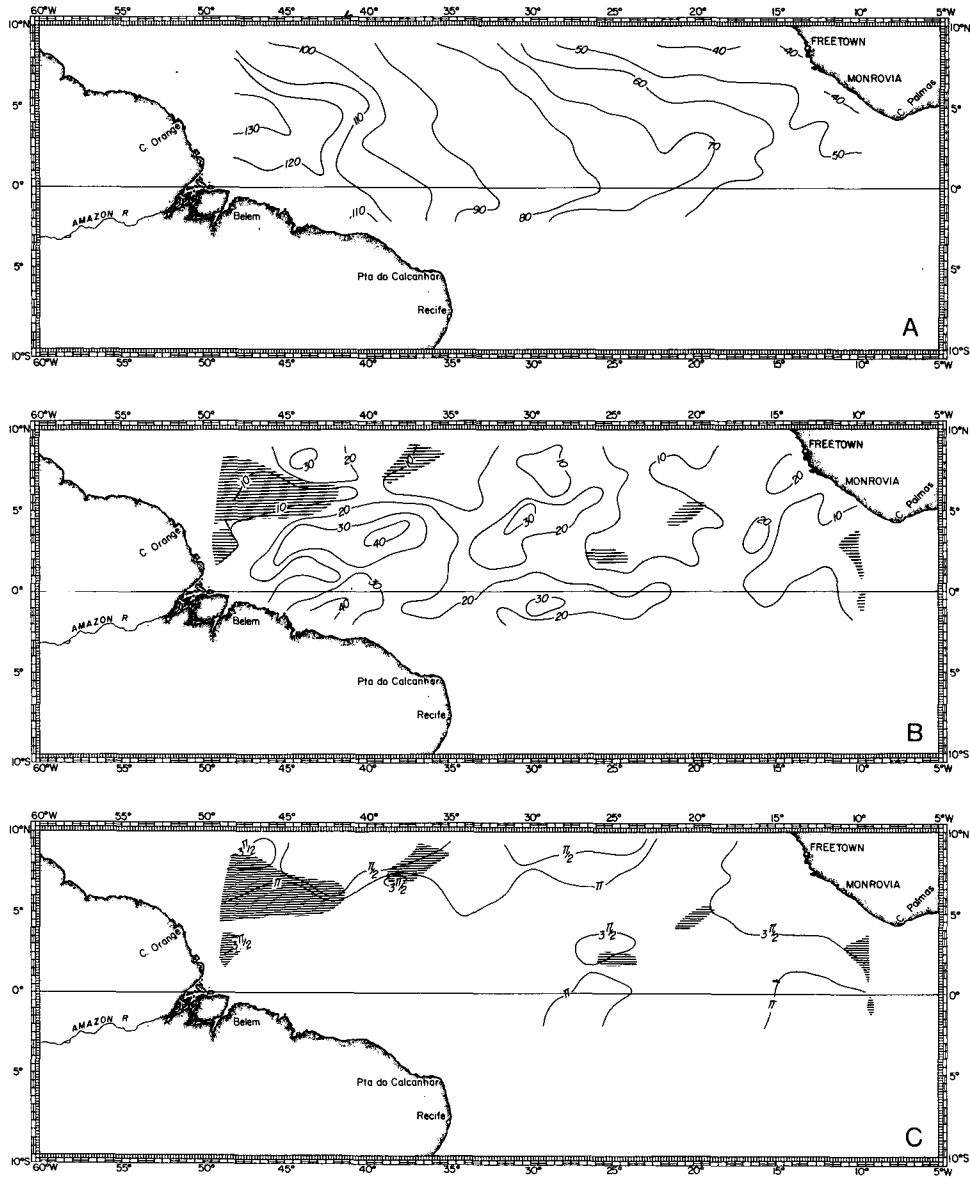
FIG. 3. (a) Annual mean of the depth of the thermocline (in meters), defined as the depth of the maximum gradient in the region 48 to 10°W, 9°N to 3°S. (b) Amplitude and (c) phase of the annual cycle of the depth of the thermocline as calculated from the annual fits. Shaded areas correspond to regions where the coefficient of determination is not significant.

$$U_t - fV = -g'h_x + \frac{1}{H_0\rho}\,\tau^{(x)}$$

$$V_t + fU = -g'h_y + \frac{1}{H_0\rho}\,\tau^{(y)}$$

$$h_t + H_0(U_x + V_y) = 0$$

where U and V denote the averaged current in the upper layer, $\tau^{(x)}$ and $\tau^{(y)}$ the components of the surface stress imposed by the wind, g' is the reduced gravity (equal to $g\Delta\rho/\rho$, where $\Delta\rho$ is the density difference between the two layers), f the Coriolis parameter, and h and H_0 are the depth and mean depth of the thermocline, respectively. From the above one easily derives the vorticity equation:

$$h_t - C_{px}h_x + \left[\frac{H_0}{f}\,U_{ty} - \frac{H_0}{f}\,V_{tx} - \frac{\beta H_0}{f^2}\,U_t\right]$$

$$= -\left(\nabla \times \frac{\tau}{f\rho_0}\right), \quad (1)$$

where $C_{px} = \beta g' H_0/f^2$ is the phase speed of propagation

for non-dispersive Rossby waves. The first term on the lhs when equated to the rhs is the vertical velocity due to Ekman divergence in the upper layer. A balance with the second term and the rhs yields a baroclinic form of the Sverdrup relation. The terms between brackets derive from the acceleration terms.

Figs. 6 and 7 show the (x, t) field for the depth of the thermocline and the curl τ/f, respectively, band-averaged in both the northern and southern region of the NECC. West of 20°W, the annual variation of the depth of the thermocline in the southern side of the NECC (4 to 7°N) fluctuates 180° out of phase with the oscillations on the northern side (7 to 10°N). East of 20°W the thermocline rises and falls nearly in phase across the NECC. The curl τ/f is qualitatively correlated to this behavior: it oscillates 180° out of phase between the northern and southern sides of the western basin and, except for a one-month lag, the general pattern is very similar to that of the ocean. This comparison
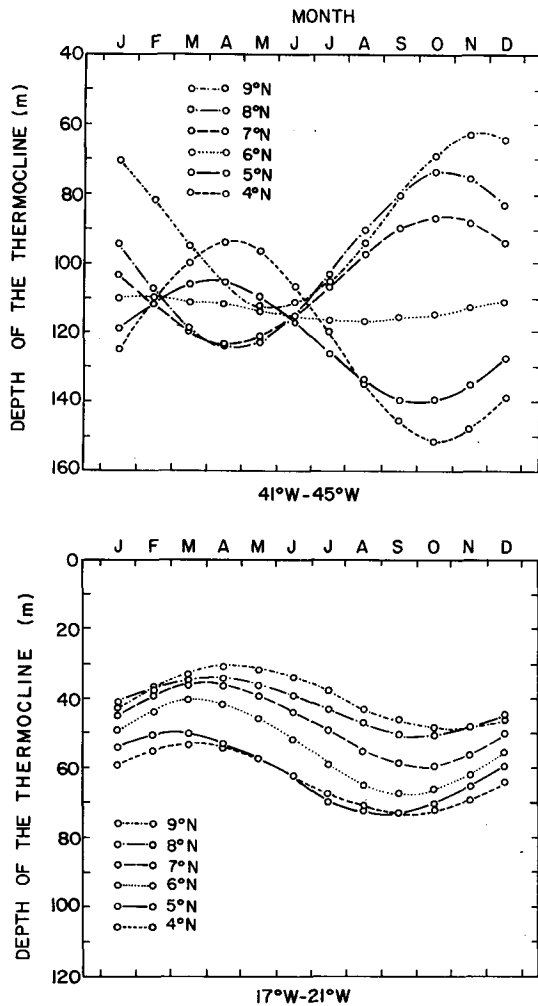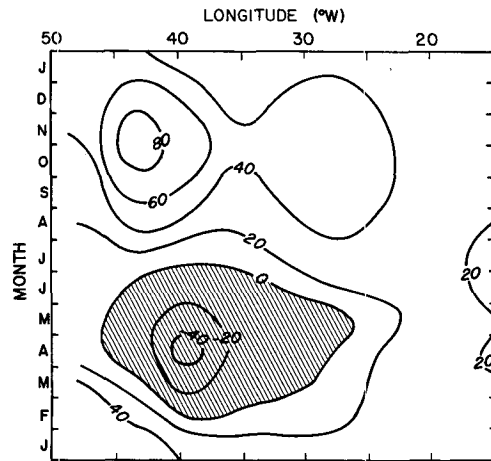

FIG. 5. Difference (north to south) in the thermocline depth across the NECC (in m) as a function of time and longitude.

suggests a strong correlation between both fields. Assuming a geostrophic balance between U, V and h as a first approximation, equation (1) becomes:

$$h_t - C_{px}h_x + \left[\frac{2H_0g'\beta}{f^3}h_{yt} - \frac{g'H_0}{f^2}h_{yyt} - \frac{H_0g'}{f^2}h_{xxt}\right]$$
$$= -(\nabla \times \tau/f\rho_0). \quad (2)$$

Using the depth of the thermocline field $h(x, y, t)$ obtained from the historical data, we calculate each one of the lhs terms of Eq. (2). The resolution used for the derivatives is: $\Delta x = 4°$, $\Delta y = 2°$, $\Delta t = $ one month. The rhs of Eq. (2) is calculated with a $2° \times 2°$ resolution. The g' varies insignificantly and has been assigned a value of 2×10^{-2} m s^{-2}. The Coriolis parameter f, its derivative β and $C_{px} = \beta g'H_0/f^2$ have been evaluated at each latitude with H_0 being the an-
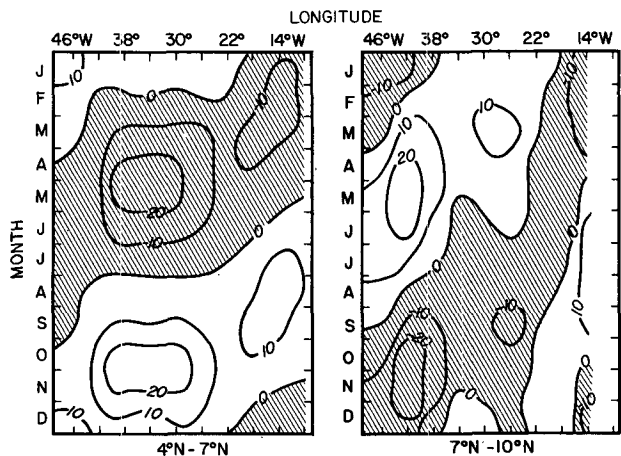

FIG. 4. Examples of the annual cycle of the thermocline depth along the Atlantic basin in the region of the NECC.

FIG. 6. Variation of the thermocline depth as a function of time and longitude for the southern (4 to 7°N) and northern (7 to 10°N) sides of the NECC. The annual mean was subtracted at each 4° longitude band. Units of meters.
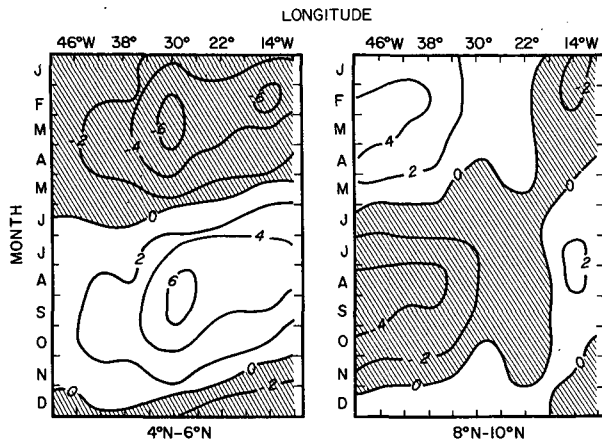
LONGITUDE

FIG. 7. Annual cycle of the curl of the wind stress ($\nabla \times \tau/f\rho_0$) as a function of latitude for the southern and northern sides of the NECC. The annual mean was subtracted at each 4° longitude band. Units of dyn cm^{-3}.

nual mean of the depth of the thermocline in the area. The equation has also been solved with H_0 being the annual mean of the thermocline at each latitude band and there is no significant difference in the results.

Figure 8 compares both sides of Eq. (2) by area. Away from the meridional continental boundaries, the two sides of the equation are typically one or two months out of phase, and there is a remainder on average of 1.5×10^{-6} m s^{-1} in magnitude that is not balanced. The significance of this difference can be measured by noting that a 4 m error in the estimate of Δh in either of the first two terms on the lhs will result in error of that magnitude (1.5×10^{-6} m s^{-1}). Recalling that we estimated the error in determining the annual variation of h at a point from the original data set to be between 3 and 8 m, we would conclude

that over a large part of the basin the vorticity equation is as balanced as these data can resolve.

The relative importance of the first two terms also varies. Figs. 9 through 12 (a and b) show some representative results along the basin. In (a) of each of the figures in the annual variations of the amplitude of each one of the terms that contribute to the lhs of the equation are shown. Part (b) of the figures compares their sum (acceleration terms included and excluded) with the annual variation of $-\nabla \times \tau/f\rho_0$ for each selected area. Three general areas can be described.

a. West of 42° W

The amplitude variations due to the Ekman pumping term (h_t) are of the same order of magnitude as the acceleration terms and all are small compared to the Sverdrup term ($-C_{px}h_x$) (Fig. 9a). This statement is valid south of 7°N. Between 7 and 9°N, h_t and $-C_{px}h_x$ are of the same order of magnitude and the acceleration terms are negligible. The vorticity equation, in the approximation we use, does not hold in this region. There is no balance between the right and left side of the equation (Fig. 9b). In particular at 4°N both terms are 180° out of phase.

b. In the center of the basin: 42 to 22° W

The Ekman pumping and the Sverdrup term are the dominant contributions. The acceleration terms are negligible (Figs. 10a and 11a).

Almost everywhere in this region the two sides are nearly balanced. Fig. 10b shows an instance where the agreement is excellent. Fig. 11b is more representative of the situation: a difference from 0 to 3×10^{-6} m s^{-1} between the annual means and a one-month phase lag.
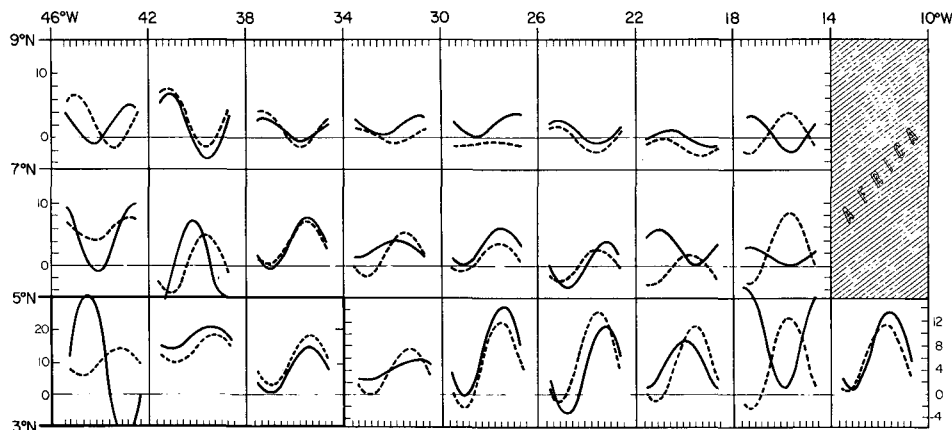

FIG. 8. Comparison between the left- and right-hand sides of Eq. (2) as calculated from the historical data for each one of the 4° × 2° boxes. The curves are (solid line) $h_t - C_{px}h_x$ and (dashed line) $-\nabla \times \tau/f\rho_0$. The abscissa is the month, beginning with January; the ordinate scale is in units of 10^{-6} m s^{-1} (note that the three lower-left panels have been doubled).

c. East of 22°W

For the region 14 to 18°W, in the central band to 22°W, the results are similar to those obtained in the western side of the basin: the Sverdrup term $(-C_{px}h_x)$ dominates, the Ekman pumping contribution (h_t) in the southern region is of the same order of magnitude as the acceleration terms (Fig. 12a) and the vorticity equation in its present form does not hold (Fig. 12b).

The magnitude of the terms in (1) has been theoretically calculated by Busalacchi and Picaut (1983). They conclude that in the northwestern region (10°N, 48°W) the effect of the acceleration terms is small, but in the southwestern region (3°N, 43°W) only the V_{xt}
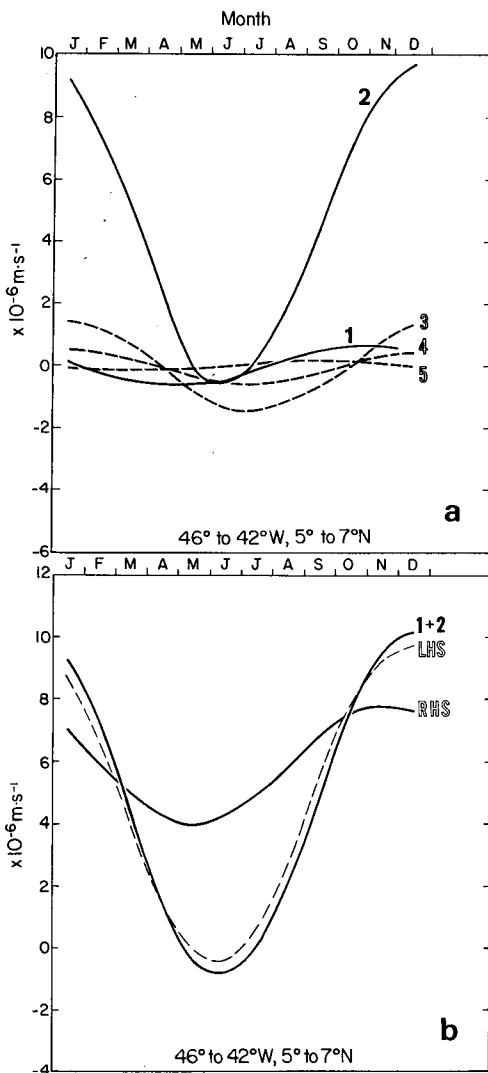

FIG. 9. (a) Annual variation of the amplitude of the different contributions to the left side of Eq. (2) for the region 46 to 42°W, 5 to 7°N. The different curves are 1) h_t, 2) $-C_{px}h_x$, 3) $-(g'H_0/f^2)h_{yyt}$, 4) $(g'H_0\beta/f^3)h_{yt}$, 5) $-(g'H_0/f^2)h_{xxt}$. (b) For the same region of (a) where $h_t - C_{px}h_x$ of Eq. (2) is curve (1 + 2), the lhs of (2) is dashed and the rhs is solid.
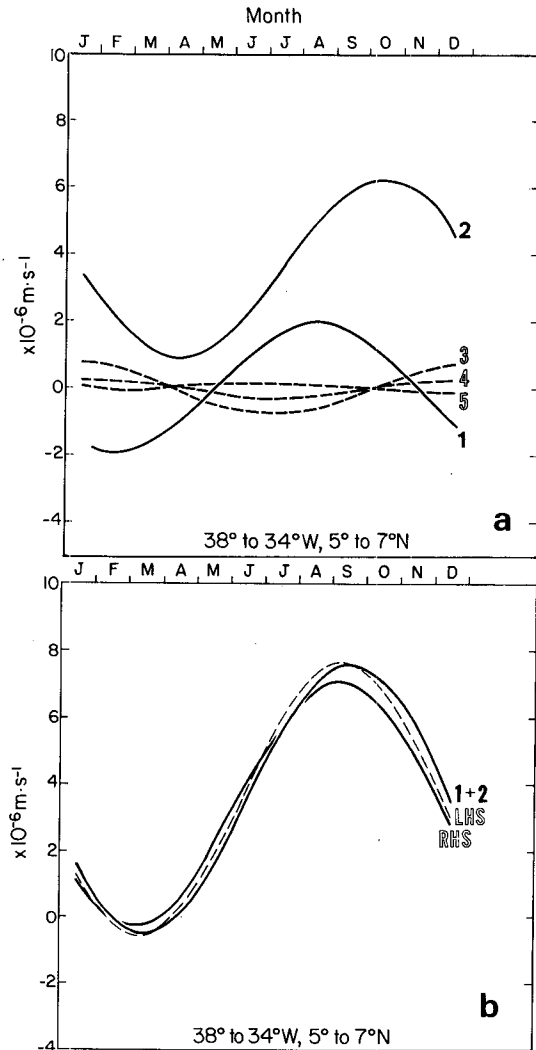

FIG. 10. (a) and (b). As in Fig. 9 but for the region 38 to 34°W, 5 to 7°N.

term can be ignored. The discrepancy between their theoretical results in the southern region and the present calculations from the data is due to the fact that their model underestimated the contribution due to the divergence of the geostrophic currents $(C_{px}h_x)$. The data show that the divergence term dominates the others by one order of magnitude and that the vorticity equation as proposed by both studies does not hold in the area.

4. Summary and conclusions

The analysis performed from the historical data allowed us to establish with some precision the period of time and the region of the equatorial Atlantic where the NECC reverses. We also find that the variability of the thermal structure is qualitatively correlated with the variability of the trade winds. West of 25°W, the
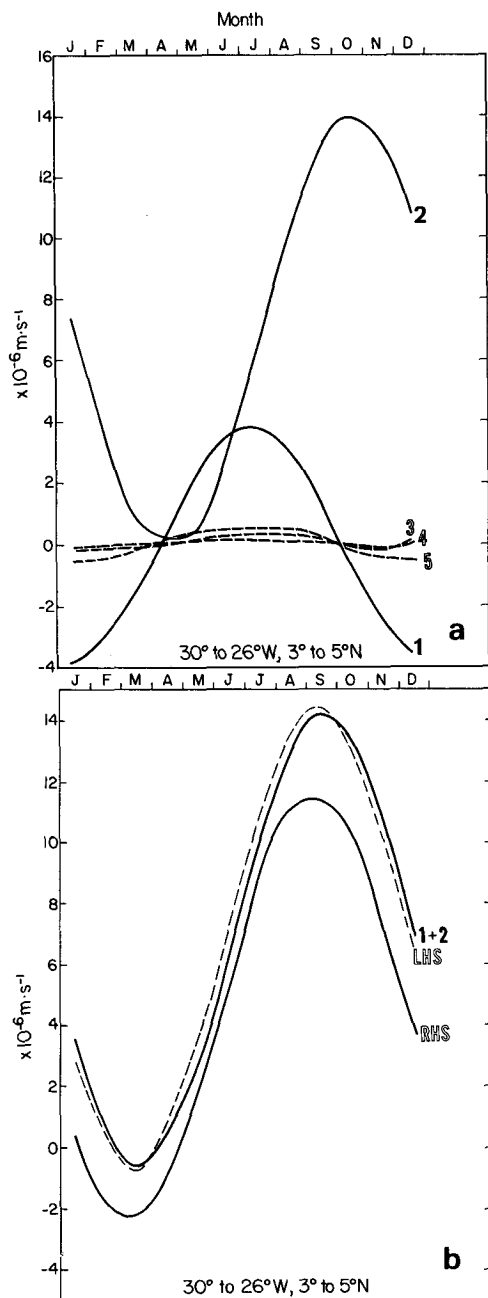
FIG. 11. (a) and (b). As in Fig. 9 but for
the region 30 to 26°W, 3 to 5°N.

structure, the NECC disappears during the boreal
spring in the western basin. The curl of the wind stress
also oscillates 180° out of phase between the northern
and southern sides of the western basin.

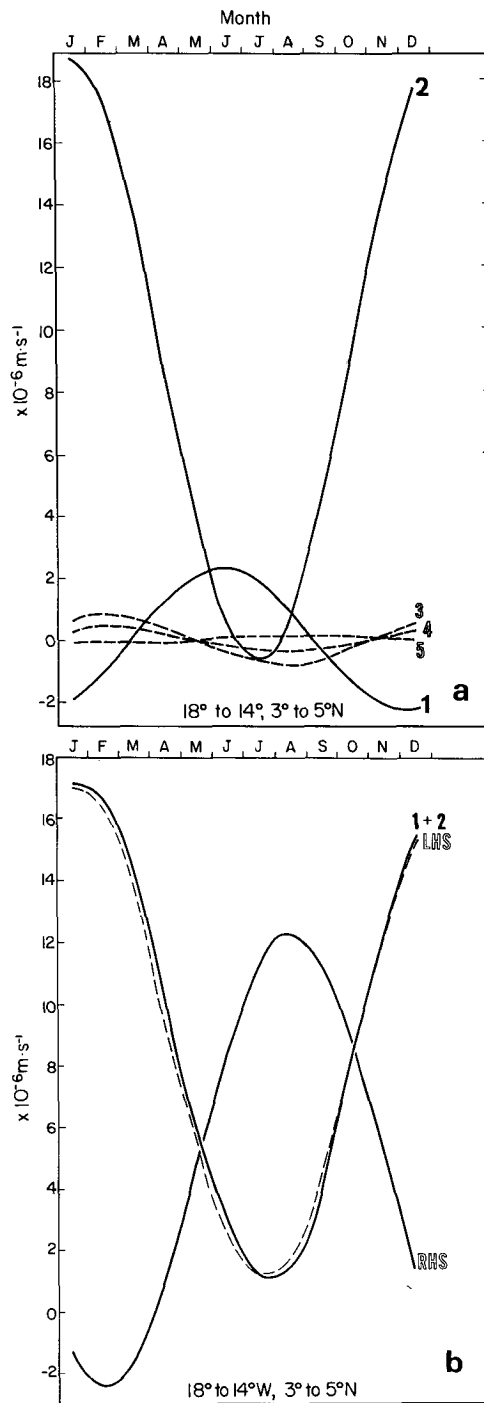A simple equation that relates the thermal structure

FIG. 12. (a) and (b). As in Fig. 9 but for
the region 18 to 14°W; 3 to 5°N.

annual variation of the depth of the thermocline in
the southern side of the NECC (4 to 7°N) fluctuates
180° out of phase of the oscillation on the northern
side (7 to 10°N). East of 25°W, the thermocline rises
and falls nearly in phase across the countercurrent.
Differences in the depth of the thermocline between
the northern and southern regions show that if the
flow can be uniquely presumed from the thermal

variations with the trade winds is the vorticity equation, which in its linear form, is given by Eq. (1). Each one of the terms has been calculated from the historical data.

From the analysis performed we conclude that the terms derived from the acceleration terms, estimated assuming geostrophy, do not contribute significantly to the thermocline displacement anywhere in the entire basin under consideration (48 to 10°W; 10 to 3°N). Their maximum contribution is attained in the southern part of the basin ($\Delta y = 5$–$3°N$) and when added are less than 10 percent of the total amplitude. If these terms contribute dynamically to the ocean's response, it must occur at time scales shorter than the seasonal changes being considered here.

Other results vary along the basin. In Fig. 8 we reported the results of the comparison between the sum of the contributions to the vorticity equation from the Ekman and Sverdrup terms with the vorticity being applied by the wind field. In the center of the basin, the results were good. The two sides of the equation are typically one or two months out of phase and there is a remainder, on average, of 1.5×10^{-6} m s^{-1} in magnitude. This imbalance is not thought to be significant considering the uncertainty in our derived data set, $h(x, y, t)$, and we conclude that the three terms are in balance at the annual frequency.

In contrast, the balance of terms breaks down significantly in the sampling areas nearest the eastern and western boundaries. The two sides of the equation are as much as six months out of phase and have different amplitudes. An explanation for the loss of balance may lie with the increasing importance of lateral diffusion as we approach the meridional boundaries or non-linear terms becoming important in the regions influenced by the presence of boundary currents.

In conclusion, in the interior of the basin, the annual cycle of the depth of the thermocline is in balance with the annual cycle of the rotational stress induced at the sea surface by the wind. The reversal of curl τ/f in the western side of the basin is therefore responsible for the reversal of the NECC.

REFERENCES

Belevich, R. R., I. M. Martynovich and N. A. Arnaut, 1979: *Hydrography and Meteorology of the Atlantic Ocean. Proc. of the State Oceanological Institute,* Vol. 150, R. R. Belevich, Ed., Moscow. The Moscow Hydrometeorology Division, 3, 20 pp.

Bubnov, V. A., and V. D. Egorikhin, 1979: Study of water calculation in the tropical Atlantic. *Deep-Sea Res.,* **26**(GATE Suppl. II), 125–136.

Busalacchi, A. J., and J. J. O'Brien, 1980: The seasonal variability in a model of the tropical Pacific. *J. Phys. Oceanogr.,* **10**, 1929–1951.

——, and J. Picaut, 1983: Seasonal variability from a model of the tropical Atlantic Ocean. *J. Phys. Oceanogr.,* **13**, 1564–1588.

Cane, M. A., and E. S. Sarachik, 1981: The response of a linear equatorial ocean to periodic forcing. *J. Mar. Res.,* **39**, 651–693.

Hellerman, S., 1980: Charts of the variability of the wind stress over the tropical Atlantic. *Deep-Sea Res.,* **26**(GATE Suppl. II), 63–75.

Katz, E. J., 1981: Dynamic topography of the sea surface in the equatorial Atlantic. *J. Mar. Res.,* **39**, 53–63.

Leetmaa, A., and A. F. Bunker, 1978: Updated charts of the mean annual wind stress, convergences in the Ekman Layers, and Sverdrup transports in the North Atlantic. *J. Mar. Res.,* **36**, 311–322.

McCreary, J., 1976: Eastern tropical ocean response to changing wind systems with application to El Niño. *J. Phys. Oceanogr.,* **6**, 632–645.

Merle, J., 1978: *Atlas Hydrologique Saisonnier de l'Ocean Atlantique Intertropical.* Travaux et documents de l'ORSTOM, No. 82, ORSTOM, Paris.

Meyers, G., 1975: Seasonal variation in transport of the Pacific North Equatorial Current relative to the wind field. *J. Phys. Oceanogr.,* **5**, 442–449.

——, 1979: On the annual Rossby Wave in the tropical North Pacific Ocean. *J. Phys. Oceanogr.,* **9**, 663–674.

White, W. B., 1977: Annual forcing of baroclinic long waves in the tropical North Pacific Ocean. *J. Phys. Oceanogr.,* **7**, 50–61.

——, 1978: A wind-driven model experiment of the seasonal cycle of the main thermocline in the interior midlatitude North Pacific. *J. Phys. Oceanogr.,* **8**, 818–824.